CALCULATION OF THE ADDED MASS AND DAMPING FORCES ON SUPERCAVITATING BODIES

Neal E. FINE and James S. UHLMAN
Applied Mechanics Department, Engineering Technology Center, Anteon Corporation
One Corporate Place, Middletown, RI 02842, USA

ABSTRACT

A linearized formulation for the unsteady forces experienced by supercavitating bodies is developed in terms of added mass and damping coefficients. The formulation is general, but is applied here using an axisymmetric base flow. Expressions for the added mass, damping and restoring tensors are derived in a form suitable for incorporation in a numerical "flight" simulation tool for supercavitating vehicles. The expressions are evaluated numerically using a low-order boundary element method for both the axisymmetric base flow and the unsteady perturbation. Disk and conical cavitating bodies are investigated. It is found that the added mass in surge and heave can be negative for small values of the disturbance frequency. The physical interpretation of this phenomenon is provided.

NOMENCLATURE

d	Cavitator diameter
F	Function in space describing the body/cavity surface
G	Greens function
i	$\sqrt{-1}$
k	Dimensionless frequency, $k = \omega d / U_0$
n	Coordinate direction normal to the body and cavity surface
p	Pressure
S	Surface area
s	Arclength, and coordinate direction tangent to the body/cavity surface
t	Time
U_0	Steady body velocity
ϕ, μ	Unsteady disturbance potentials
Φ	Total velocity potential
ρ_0	Fluid density
σ	Cavitation Number $\sigma = 2(p_\infty - p_c)/\rho_0 U_0^2$
ω	Disturbance frequency
$\vec{x}$	Boundary displacement vector, $x = \lvert\vec{x}\rvert$

Subscripts:

0	Indicates steady basis flow (e.g., Φ_0)
BW	Refers to the wetted body surface for the nominal steady conditions (e.g., S_{BW})
C, c	Indicates a cavity parameter (e.g., S_C, p_c)
i, j	Indices indicating the direction of unsteady motion (e.g., i=1 for surge, 2 for sway, etc)
J	Indicates a re-entrant jet parameter (e.g., S_J)

INTRODUCTION

Current interest in the development of supercavitating high-speed vehicles has led to the development of guidance and control algorithms for supercavitating bodies (Kirschner, et al, 2001). Unfortunately, incorporation of added mass effects in the equations of motion of supercavitating bodies is complicated by the fact that the shape and extent of the cavity boundary depends on the history of the body motion. Unlike fully-wetted flows, the added mass force experienced by supercavitating bodies depends on the history of the body motion.

In this work, we seek to quantify the unsteady forces experienced by supercavitating bodies in an irrotational flow of an inviscid and incompressible fluid. By defining an added mass tensor for supercavitating vehicles, we hope to find a simple and accurate approach to including unsteady inertial forces in their equations of motion. Our approach is to formulate the unsteady problem as a perturbation of a steady basis flow, and to solve for the unsteady flow in the frequency domain. This approach bears great similarity to that taken in previous works in solving the problem of ship motions in a seaway. For that reason, the formulation presented here follows two seminal works on that subject: Timman and Newman (1962) and Ogilvie and Tuck (1969).

1. PROBLEM STATEMENT

Consider a supercavitating body, such as the one shown in figure 1, moving with steady velocity U_0 in the negative x direction. We seek expressions for the added mass and damping forces experienced by the body in response to unsteady motions, which will be assumed to be small relative to the forward speed. We will formulate the boundary value problem using a Cartesian coordinate

system $\vec{x} = (x, y, z)$ fixed on the vehicle. The fluid is assumed to be inviscid and incompressible and the flow irrotational, so that the velocity field may be written as the gradient of a potential, $\Phi(\vec{x}, t)$, which satisfies Laplace's equation:

$$\nabla^2\Phi = 0 . \tag{1}$$

The total fluid velocity is described as an unsteady perturbation superposed on a steady mean flow. Accordingly, the velocity potential is decomposed into a steady mean velocity potential and an unsteady perturbation potential:

$$\Phi(\vec{x}, t) = \Phi_0(\vec{x}) + f(\vec{x}, t) . \tag{2}$$

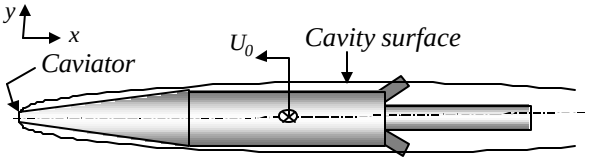

Figure 1. Notional sketch of a supercavitating vehicle.

1. 1 Kinematic Boundary Condition

If the body and cavity surfaces are represented by the function $F(\vec{x}, t)$, then the exact kinematic boundary condition to be satisfied on the surface is:

$$\frac{DF}{Dt} = \frac{\partial F}{\partial t} + \nabla(\Phi_0 + f)\cdot\nabla F = 0 . \tag{3}$$

The position of the surface may be defined as the sum of the steady mean position, $\vec{x}_0 = (x_0, y_0, z_0)$, and a small unsteady displacement:

$$\vec{x} = \vec{x}_0 + \vec{x}(\vec{x}_0, t) . \tag{4}$$

Using this definition, the time derivative and gradient of F may be written as follows:

$$\frac{\partial F}{\partial t} = -\frac{\partial \vec{x}}{\partial t}\cdot\nabla_{x_0} F$$

$$\nabla F = \nabla_{x_0} F - \hat{i}\frac{\partial \vec{x}}{\partial x_0}\cdot\nabla_{x_0} F - \hat{j}\frac{\partial \vec{x}}{\partial y_0}\cdot\nabla_{x_0} F - \hat{k}\frac{\partial \vec{x}}{\partial z_0}\cdot\nabla_{x_0} F$$

where the subscript "x_0" denotes that the gradient operator is to be evaluated on the mean position of the body, with $\vec{x} = \vec{x}_0$. The unit vectors in the x_0, y_0 and z_0 coordinate directions are $\hat{i}, \hat{j}$ and $\hat{k}$, respectively. Substituting these expressions in equation (3), the kinematic boundary condition becomes:

$$-\frac{\partial \vec{x}}{\partial t}\cdot\nabla_{x_0} F + \nabla(\Phi_0 + f)\cdot \left(\nabla_{x_0} F - \hat{i}\frac{\partial \vec{x}}{\partial x_0}\cdot\nabla_{x_0} F - \hat{j}\frac{\partial \vec{x}}{\partial y_0}\cdot\nabla_{x_0} F - \hat{k}\frac{\partial \vec{x}}{\partial z_0}\cdot\nabla_{x_0} F\right) = 0 \tag{5}$$

Equation (5) applies on the exact body surface $F(\vec{x}, t)$. Following Timman and Newman (1962), this expression may be linearized under the assumption that the unsteady displacement amplitudes, the perturbation potential and its spatial derivatives are all small. Using a Taylor expansion for the velocity field

$$\nabla(\Phi_0 + f) = \nabla_{x_0}\Phi_0 + \vec{x}\cdot\nabla_{x_0}(\nabla_{x_0}\Phi_0) + \nabla_{x_0} f + O(x^2) \tag{6}$$

we may recast equation (5) as follows:

$$-\frac{\partial \vec{x}}{\partial t}\cdot\nabla_{x_0} F + \left(\nabla_{x_0}\Phi_0 + \vec{x}\cdot\nabla_{x_0}(\nabla_{x_0}\Phi_0) + \nabla_{x_0} f\right)\cdot \left(\nabla_{x_0} F - \hat{i}\frac{\partial \vec{x}}{\partial x_0}\cdot\nabla_{x_0} F - \hat{j}\frac{\partial \vec{x}}{\partial y_0}\cdot\nabla_{x_0} F - \hat{k}\frac{\partial \vec{x}}{\partial z_0}\cdot\nabla_{x_0} F\right) + O(x^2) = 0. \tag{7}$$

Rearranging terms, the unsteady components of equation (7) become:

$$\nabla_{x_0} f\cdot\nabla_{x_0} F = \frac{\partial \vec{x}}{\partial t}\cdot\nabla_{x_0} F + \left(\nabla_{x_0}\Phi_0\cdot\nabla_{x_0}\vec{x} - \vec{x}\cdot\nabla_{x_0}(\nabla_{x_0}\Phi_0)\right)\cdot\nabla_{x_0} F + O(x^2) \tag{8}$$

Noting that $\nabla_{x_0} F$ is normal to the body/cavity surface, equation (8) reduces to

$$\frac{\partial f}{\partial n} = \frac{\partial \vec{x}}{\partial t}\cdot\hat{n} + \left(\nabla_{x_0}\Phi_0\cdot\nabla_{x_0}\vec{x} - \vec{x}\cdot\nabla_{x_0}(\nabla_{x_0}\Phi_0)\right)\cdot\hat{n} \tag{9}$$

Equation (9) is the linearized kinematic boundary condition which, consistent with the linearization, can be applied on the mean body/cavity surface.

We now consider only the wetted portion of the boundary and assume that its motion is associated with rigid-body motion of the vehicle. The displacement amplitude may be expressed as the sum of a rigid body translation, $\vec{x}_T$, and rotation, $\vec{x}_R$:

$$\vec{x} = \vec{x}_T + \vec{x}_R\times\vec{x}_0 . \tag{10}$$

Decomposing the perturbation potential into a sum of components proportional to complex harmonic displacement amplitudes,

$$f = z_j j_j(\vec{x}_0) e^{iwt} \tag{11}$$

where summation over repeated indices is implied and where the magnitudes of the complex amplitudes are

$$\begin{aligned}(z_1, z_2, z_3) e^{iwt} &= \vec{x}_T \\ (z_4, z_5, z_6) e^{iwt} &= \vec{x}_R,\end{aligned} \tag{12}$$

and substituting equation (11) in equation (9) yields

$$\frac{\partial j_j(\vec{x}_0)}{\partial n} = iwn_j + m_j \tag{13}$$

where the generalized normal and so-called "m-terms" are given by (Ogilvie and Tuck, 1969) as

$$\begin{aligned}(n_1, n_2, n_3) &= \hat{n} \\ (n_4, n_5, n_6) &= \vec{x}_0 \times \hat{n} \\ (m_1, m_2, m_3) &= -\hat{n} \cdot \nabla_{x_0} \left(\nabla_{x_0} \Phi_0(\vec{x}_0) \right) \\ (m_4, m_5, m_6) &= -\hat{n} \cdot \nabla_{x_0} \left(\vec{x}_0 \times \nabla_{x_0} \Phi_0(\vec{x}_0) \right).\end{aligned} \tag{14}$$

Equation (13) is the linearized kinematic boundary condition to be applied on the wetted portion of the body for each mode of oscillation, j=1,..,6 (see figure 2).

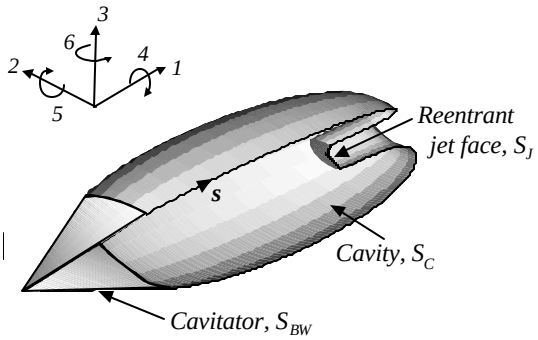

Figure 2. Cut-away sketch of a supercavitating cone showing the various surface definitions.

1.2 Dynamic Boundary Condition

To derive the linearized dynamic boundary condition, we start with the following form of Bernoulli's equation:

$$r_0 \frac{\partial \Phi(\vec{x}, t)}{\partial t} + \tfrac{1}{2} r_0 \nabla \Phi(\vec{x}, t) \cdot \nabla \Phi(\vec{x}, t) = (p_\infty - p_c) + \tfrac{1}{2} r_0 U_0^2 \tag{15}$$

where p_∞ and p_c are the pressures at infinity and in the cavity, respectively, and where gravity effects are ignored. Inserting the decomposition of the total potential given in equation (2) and the Taylor expansion of its gradient from equation (6), this becomes:

$$\begin{aligned}&2 \frac{\partial f(\vec{x}_0, t)}{\partial t} + \\ &\left(\nabla_{x_0} \Phi_0(\vec{x}_0) + \vec{x} \bullet \nabla_{x_0} (\nabla_{x_0} \Phi_0(\vec{x}_0)) + \nabla_{x_0} f(\vec{x}_0, t) \right) \bullet \\ &\bullet \left(\nabla_{x_0} \Phi_0(\vec{x}_0) + \vec{x} \bullet \nabla_{x_0} (\nabla_{x_0} \Phi_0(\vec{x}_0)) + \nabla_{x_0} f(\vec{x}_0, t) \right) \\ &= U_0^2 (1 + s)\end{aligned} \tag{16}$$

where the cavitation number is defined as follows:

$$s = \frac{p_\infty - p_c}{\frac{1}{2} r_0 U_0^2}.$$

Keeping only terms linear in x, equation (16) reduces to

$$\begin{aligned}&2 \frac{\partial f(\vec{x}_0, t)}{\partial t} + \\ &\nabla_{x_0} \Phi_0(\vec{x}_0) \bullet \nabla_{x_0} \Phi_0(\vec{x}_0) + 2 \nabla_{x_0} \Phi_0(\vec{x}_0) \bullet \nabla_{x_0} f(\vec{x}_0, t) \\ &+ 2 \nabla_{x_0} \Phi_0(\vec{x}_0) \bullet \left(\vec{x} \bullet \nabla_{x_0} (\nabla_{x_0} \Phi_0(\vec{x}_0)) \right) = U_0^2 (1 + s)\end{aligned} \tag{17}$$

The steady potential, $\Phi_0(\vec{x}_0)$, is assumed to satisfy the steady dynamic boundary condition:

$$\nabla_{x_0} \Phi_0(\vec{x}_0) \bullet \nabla_{x_0} \Phi_0(\vec{x}_0) = U_0^2 (1 + s) \quad \text{on the cavity} \tag{18}$$

so that equation (17) reduces to

$$\begin{aligned}&\frac{\partial f(\vec{x}_0, t)}{\partial t} + \nabla_{x_0} \Phi_0(\vec{x}_0) \bullet \nabla_{x_0} f(\vec{x}_0, t) \\ &\quad + \nabla_{x_0} \Phi_0 \bullet \left(\vec{x} \bullet \nabla_{x_0} \left(\nabla_{x_0} \Phi_0(\vec{x}_0) \right) \right) = 0\end{aligned} \tag{19}$$

The last term on the left-hand-side of equation (19) may be evaluated as follows:

$$\begin{aligned}\nabla_{x_0} \Phi_0 \bullet \left(\vec{x} \bullet \nabla_{x_0} (\nabla_{x_0} \Phi_0) \right) &= \vec{x} \bullet \left(\nabla_{x_0} (\nabla_{x_0} \Phi_0) \bullet \nabla_{x_0} \Phi_0 \right) \\ &= \tfrac{1}{2} \vec{x} \bullet \nabla_{x_0} \left(\nabla_{x_0} \Phi_0 \bullet \nabla_{x_0} \Phi_0 \right) \\ &= 0\end{aligned} \tag{20}$$

This term vanishes on S_C because the last bracketed term of (20) is constant, according to equation (18).

Substituting the decomposition of the perturbation potential, equation (11), in equation (19) and making use of equation (20) results in the following linearized dynamic boundary condition:

$$iwj_j(\vec{x}_0) + \nabla \Phi_0(\vec{x}_0) \bullet \nabla j_j(\vec{x}_0) = 0. \tag{21}$$

Equation (21) will be applied on the steady mean cavity surface, S_C, for all six degrees of freedom (j=1,…,6).

1.3 Cavity Termination

The need for a termination model arises from the inconsistency inherent in forcing a constant-pressure streamline to end at a stagnation point. In this effort, a re-entrant jet cavity termination model is employed, as shown in figure 2. This termination model was originally devised by Efros (1946) and Kreisel (1946), and is motivated by experimental observation. Details of the numerical implementation in the boundary element method may be found in Uhlman (2001).

1.4 Boundary Integral Equation

The perturbation potential satisfies Green's third identity:

$$2p f(\vec{x},t) + \iint_S \left[f(\vec{y},t)\frac{\partial}{\partial n}\big(G(\vec{x},\vec{y})\big) - G(\vec{x},\vec{y})\frac{\partial}{\partial n}\big(f(\vec{y},t)\big)\right] dS = 0 \tag{22}$$

where the Green's function, G, is given by

$$G(\vec{x},\vec{y}) = \frac{1}{|\vec{x}-\vec{y}|} \tag{23}$$

and where the field point, $\vec{x}$, lies on the boundary. Substituting the decomposition (11) and noting that the complex amplitudes, z_j, have no spatial dependence, we find that each complex potential, j_j, satisfies

$$2p j_j(\vec{x}) + \iint_S \left[j_j(\vec{y})\frac{\partial G(\vec{x},\vec{y})}{\partial n} - G(\vec{x},\vec{y})\frac{\partial j_j(\vec{y})}{\partial n}\right] dS = 0 \tag{24}$$

The boundary conditions to be satisfied are the kinematic boundary condition (equation (13)), which defines the source distribution $\partial j_j / \partial n$ on the wetted portion of the body, and the dynamic boundary condition (equation (21)) which may be used to define the dipole distribution j_j on the cavity. Inserting the kinematic boundary condition in (24) and rearranging terms so that the known quantities are on the right-hand-side, we arrive at the following expression:

$$\begin{aligned} 2p j_j + \iint_{S_{BW}} j_j(\vec{y})\frac{\partial G(\vec{x},\vec{y})}{\partial n} dS - \iint_{S_C+S_J} \frac{\partial j_j(\vec{y})}{\partial n} G(\vec{x},\vec{y}) dS \\ + \iint_{S_C+S_J} j_j(\vec{y})\frac{\partial G(\vec{x},\vec{y})}{\partial n} dS \\ = \iint_{S_{BW}} \{ iw n_j + m_j \} G dS \end{aligned} \tag{25}$$

Here, the wetted body surface is S_{BW}, the cavity surface is S_C and the jet face is S_J, as shown in figure 2. Note that the potential on the cavity and jet may be determined by numerically integrating equation (21). This will be described in more detail in the context of an axisymmetric basis flow in Section 2.

1.5 Hydrodynamic Coefficients

Once the source and dipole distributions have been computed, the forces may be found by integrating the pressure over the wetted surface

$$F_i(t) = \iint_{S_B(t)} p(\vec{x},t) n_i dS \ . \tag{26}$$

In (26), $S_B(t)$ is the exact surface of the body. The unsteady pressure on $S_B(t)$ may be written

$$\begin{aligned} p(\vec{x},t) = -r_0 \frac{\partial}{\partial t}\big(f(\vec{x},t)\big) \\ -\tfrac{1}{2} r_0 \nabla\big(\Phi_0(\vec{x}) + f(\vec{x},t)\big)\bullet\nabla\big(\Phi_0(\vec{x}) + f(\vec{x},t)\big) \end{aligned} \tag{27}$$

If we again introduce the intermediate coordinate system, $\vec{x}_0$, as in (4), equation (27) may be linearized for small x as follows:

$$\begin{aligned} p(\vec{x}_0,t) = -r_0 \frac{\partial}{\partial t}\big(f(\vec{x}_0,t)\big) - r_0 \nabla_{x_0}\Phi_0(\vec{x}_0)\bullet\nabla_{x_0} f(\vec{x}_0,t) \\ -\tfrac{1}{2} r_0 \vec{x}\bullet\nabla_{x_0}\left(\nabla_{x_0}\Phi_0(\vec{x}_0)\bullet\nabla_{x_0}\Phi_0(\vec{x}_0)\right) \end{aligned} \tag{28}$$

For the remainder of this paper, there will be no need to distinguish between the coordinates $\vec{x}$ and $\vec{x}_0$. It will be implicitly assumed that all quantities are defined relative to the steady mean coordinate system, $\vec{x}_0$.

Inserting the decomposition (11) in (28) and the resulting expression in (26) then yields the following equation for the force as a function of frequency (Nakos and Sclavounos, 1990):

$$F_i(w) = \mathrm{Re}\left\{ e^{iwt}\left[x_j\left(w^2 a_{ij} - iw b_{ij} - c_{ij}\right)\right]\right\} \tag{29}$$

where

$$a_{ij} = -\frac{r_0}{w^2}\mathrm{Re}\left\{ \iint_{S_{BW}} \left[iw j_j + \frac{\partial\Phi_0}{\partial x_k}\frac{\partial j_j}{\partial x_k}\right] n_i dS \right\} \tag{30}$$

$$b_{ij} = \frac{r_0}{w}\mathrm{Im}\left\{ \iint_{S_{BW}} \left[iw j_j + \frac{\partial\Phi_0}{\partial x_k}\frac{\partial j_j}{\partial x_k}\right] n_i dS \right\} \tag{31}$$

$$c_{ij} = r_0 \mathrm{Re}\left\{ \iint_{S_{BW}} \frac{\partial}{\partial x_j}\left(\frac{1}{2}\frac{\partial\Phi_0}{\partial x_k}\frac{\partial\Phi_0}{\partial x_k}\right) n_i dS \right\} \tag{32}$$

In equation (29), the force is written as a sum of added mass (a_{ij}), damping (b_{ij}) and restoring force (c_{ij}) tensors.

2. NUMERICAL IMPLEMENTATION FOR AN AXISYMMETRIC BASE FLOW

To this point, we have formulated the problem in terms of a general steady basis flow. To demonstrate the method, we now define our steady basis flow to be that of an axisymmetric cavitator with a reentrant jet cavity termination, as shown in figure 2. The steady axisymmetric flow is computed numerically via a low-order boundary element method (Uhlman, 2001). In the numerical solution of the basis flow, the cavity length is assumed to be known, and the cavitation number is determined as part of the solution. An iterative method is used to determine the cavity shape that satisfies the exact kinematic and dynamic boundary conditions.

2.1 Dynamic Boundary Condition

Noting that for an axisymmetric base problem we have

$$\nabla\Phi_0 = \frac{\partial\Phi_0}{\partial s}\hat{s} = U_0\sqrt{1+s}\,\hat{s} \text{ on } S_C \tag{33}$$

where s and $\hat{s}$ are the arclength and unit tangent vector along a meridian, we find that the dynamic boundary condition on S_C (equation (21)) becomes:

$$iw\boldsymbol{j}_j + U_0\sqrt{1+s}\,\frac{\partial \boldsymbol{j}_j}{\partial s} = 0 \text{ on } S_C. \tag{34}$$

Equation (34) is a first order ordinary differential equation for $\boldsymbol{j}_j$ and may be integrated to yield

$$\boldsymbol{j}_j = \boldsymbol{j}_{j_0} e^{-ig(s-s_0)} \tag{35}$$

where

$$g(s-s_0) = \frac{w}{U_0\sqrt{1+s}}(s-s_0) \tag{36}$$

and where $\boldsymbol{j}_{j_0}$ is the value of $\boldsymbol{j}_j$ at $s = s_0$ and s_0 is the arclength at the trailing edge of the body. The dynamic boundary condition on the jet cross section is

$$iw\boldsymbol{j}_j + \frac{\partial\Phi_0}{\partial n}\frac{\partial \boldsymbol{j}_j}{\partial n} = 0 \text{ on } S_J. \tag{37}$$

Noting that, on the jet cross section,

$$\partial\Phi_0/\partial n = U_0\sqrt{1+s},$$

equation (37) becomes

$$\frac{\partial \boldsymbol{j}_j}{\partial n} = -\frac{iw}{U_0\sqrt{1+s}}\boldsymbol{j}_{j_0} e^{-ig(s_{J_0}-s_0)} \tag{38}$$

where s_{J_0} is the arclength along the cavity to the edge of the jet cross section and where we've assumed that $\partial \boldsymbol{j}_j/\partial s$ is zero on the jet face.

2.2 Boundary Integral Equation

On the wetted part of the body, S_{BW}, Green's third identity becomes:

$$\begin{aligned} &2p\boldsymbol{j}_j + \int_{S_{BW}} \boldsymbol{j}_j \frac{\partial\Psi}{\partial n}ds' - \int_{S_C} \frac{\partial \boldsymbol{j}_j}{\partial n}\Psi ds' \\ &\quad + \boldsymbol{j}_{j_0}\left\{\int_{S_C+S_J} e^{-ig(s'-s_0)}\frac{\partial\Psi}{\partial n}ds' + \frac{ike^{-ig(s_{J_0}-s_0)}}{d\sqrt{1+s}}\int_{S_J}\Psi ds'\right\} \\ &\quad = \int_{S_{BW}}\left\{iwn_j + m_j\right\}\Psi ds' \end{aligned} \tag{39}$$

and on the cavity

$$\begin{aligned} &2p\boldsymbol{j}_{j_0}e^{-ig(s-s_0)} + \int_{S_{BW}} \boldsymbol{j}_j \frac{\partial\Psi}{\partial n}ds' - \int_{S_C} \frac{\partial \boldsymbol{j}_j}{\partial n}\Psi ds' \\ &\quad + \boldsymbol{j}_{j_0}\left\{\int_{S_C+S_J} e^{-ig(s'-s_0)}\frac{\partial\Psi}{\partial n}ds' + \frac{ike^{-ig(s_{J_0}-s_0)}}{d\sqrt{1+s}}\int_{S_J}\Psi ds'\right\} \\ &\quad = \int_{S_{BW}}\left\{iwn_j + m_j\right\}\Psi ds' \end{aligned} \tag{40}$$

where s_{BW}, s_C and s_J are the arclength domains on the wetted body, cavity and reentrant jet face. s_{J0} is the arclength at the edge of the jet. d is the body diameter at the cavity detachment location, and k is the dimensionless frequency, $k = wd/U_0$. The integrals in arclength along the meridian are computed by the boundary element method, wherein the source and dipole distributions ($\boldsymbol{j}_j$ and $\partial \boldsymbol{j}_j/\partial n$, respectively) are assumed to be constant over each arclength segment (or panel). The induced potentials, Ψ and $\partial\Psi/\partial n$, are then integrated over each panel using Guassian quadrature. Following Hess and Smith (1966) and Uhlman (2001), the source potential

$$\Psi(\vec{x},\vec{y}) = \int_{-p}^{p}\frac{1}{|\vec{x}-\vec{y}|}\,r\,dq$$

and the dipole potential

$$\frac{\partial\Psi}{\partial n}(\vec{x},\vec{y}) = \int_{-p}^{p}\frac{\partial}{\partial n_x}\left(\frac{1}{|\vec{x}-\vec{y}|}\right)r\,dq$$

may be written in terms of complete elliptic integrals of the first and second kinds. A cylindrical coordinate system is used in which r is the radius of the axisymmetric body at the plane of integration. For further details, see Appendix A. The Appendix also presents the derivation of modified source and dipole influence functions for use when there is a crossflow component to the inflow, as is the case when the motion includes pitch/yaw and heave/sway.

2.4 Results

In this section, we present added mass and damping results for the circular disk, conical cavitators with various half-angles, and a roundnose cavitator. For the present paper, we consider only surge and heave motions. Results for pitch oscillations will be presented in a separate publication.

Figure 3 shows the convergence of the added mass for a roundnose cavitator in surge with increasing number of panels. The shape of the cavitator is shown in figure 3a and the convergence is shown in figure 3b. The total number of panels used to discretize the boundary is NBOD+NCAV+NJET, where NBOD is the number of panels on the cavitator, NCAV is the number of panels representing the cavity, and NJET is the number of panels representing the jet face. The steady cavity length is five cavitator base diameters, corresponding to a cavitation number of $s \approx 0.19$. The corresponding convergence of the cavitation number is also shown in the figure.

Figure 4 shows the surge added mass and damping for the circular disk as a function of dimensionless frequency. This result demonstrates that the added mass levels off to a value close to half the theoretical value for the fully wetted disk at high frequency. A surprising aspect of the result presented in figure 4 is the fact that the added mass takes on negative values for a range of frequencies ($k \lesssim 3$). This result will be discussed in Section 2.5.

Figure 5 shows the added mass and damping for conical cavitators with half-angles of 30º, 45º and 60º, as well the results for the circular disk. The steady cavity length for each case is L/d=5.0, and the corresponding cavitation numbers are 0.183, 0.217 0.241, and 0.268, respectively. Note that, similar to the results for the disk, the added mass is negative for small reduced frequencies. However, as the half-angle increases, the level of the negative added mass decreases. For clarity, the added mass has been multiplied by the ratio $k^2/1+k^2$ in figure 5.

Figure 6 shows the added mass and damping for the same set of conical cavitators undergoing heave oscillations. As with surge, the added mass appears to asymptote to a constant at high reduced frequency, and is negative at low reduced frequencies. The magnitude of both the added mass and damping coefficients are much lower for heave than for surge.

2.5 Discussion

As shown in figure 4, the added mass in surge can take on negative values over a range of reduced frequencies. This result is surprising, since it implies that the added mass force can reinforce the motion of the body. The result is also important, since the occurrence of negative added mass can effect the stability of a high speed supercavitating vehicle.

The physical explanation of the phenomenon is as follows. When the cavitator moves in oscillatory surge, vorticity is shed at the base of the cavitator with every half-cycle of motion. The vorticity is then advected along the cavity boundary and out of the fluid domain via the reentrant jet. At any given moment, each element of shed vorticity on the cavity boundary induces an axial velocity at the cavitator in a direction that either opposes or coincides with the direction of motion of the cavitator. The axial velocity induced by the vorticity shed during the current half-cycle of motion coincides with the direction of motion. For low frequency motions, the most recent element of shed vorticity contributes most of the induced velocity. Therefore, the net induced velocity contributes to the acceleration of the fluid, resulting in a negative added mass. However, for high frequency motions, the wavelength of the sinusoidally varying vorticity is much smaller, so that the net induced axial velocity over the cavitator is greatly reduced. At high reduced frequencies there is almost no net induced axial velocity and the added mass is positive as expected.

It should be noted that an analogous phenomenon occurs for fully-wetted hydrofoils undergoing small oscillatory heave motions. In that case, the shed vorticity is advected along the wake of the foil and induces a net vertical velocity in the direction of motion. This behavior is evident in the classical Theodorsen linear theory for unsteady hydrofoil motion (see e.g., Newman, 1986). See Appendix C for more discussion of the Theodorsen problem.

CONCLUSIONS AND FUTURE WORK

A method for computing the force coefficients for supercavitating bodies undergoing oscillatory motion has been described. The method assumes small harmonic oscillations and solves a linearized boundary value problem in the frequency domain for small perturbations to a steady basis flow. The method has been demonstrated for unsteady surge and heave of axisymmetric cavitators. The numerical solution has been found to converge with increasing number of panels. It has been found that the surge added mass of the circular disk asymptotes to approximately half the theoretical value for fully wetted disks at high reduced frequencies. At low reduced frequencies, however, the added mass is actually negative. The physical explanation for this phenomenon is discussed.

Future work will include demonstrating the method for oscillating pitch motions and assessing the impact of the unsteady forces on the motions of various notional supercavitating geometries. Also, we will examine the limits of the theory for large amplitude and low frequency motions. Finally, we will apply the theory to partially cavitating bodies, and to 2D supercavitating hydrofoils.

ACKNOWLEDGEMENTS

The authors greatly appreciate the financial support of Dr. Kam Ng (Office of Naval Research) who funded this exploratory development effort under Navy contracts N00014-00-C-0182 and N00014-02-C-0218. Members of Anteon's Fluid Mechanical Systems Group, including Dr. David Kring and Mr. Benjamin Rosenthal, contributed to this research.

REFERENCES

Abramowitz, M. and I. A. Stegun (1964), Handbook of Mathematical Functions with Formulas, Graphs and Mathematical Tables, National Bureau of Standards Applied Math Series 55.

Efros, A. G. (1946), "Hydrodynamic Theory of Two-Dimensional Flow with Cavitation", *Dokl. Acad. Nauk. SSSR*, 51, pp 267-270.

Hess, J.L. and A.M.O. Smith (1966), "Calculation of Potential Flow about Arbitrary Bodies," Progress in Aeronautical Sciences, Vol. 8, Pergamon Press, New York, NY.

Kirschner, I.N. , N.E. Fine, J.S. Uhlman and D.C. Kring (2001) , "Numerical Modeling of Supercavitating Flows", RTO AVT/VKI Special Course in Supercavitating Flows, Feb. 12-16.

Kreisel, G. (1946), "Cavitation with Finite Cavitation Numbers", Technical Report No. R1/H/36, Admiralty Res. Lab.

Nakos, D. E. and P.D. Sclavounos (1990), "Ship Motions by a Three Dimensional Rankine Panel Method", *18th Naval Hydrodynamics Conference, Ann Arbor, MI*.

Newman, J.N. (1986), Marine Hydrodynamics, MIT Press, Cambridge, MA.

Ogilvie, T.F. and E.O. Tuck, (1969), "A Rational Strip Theory for Ship Motions – Part I", Report No. 013, Dept. of Naval Architecture and Marine Engineering, University of Michigan, USA.

Timman, R. and J.N. Newman, (1962), "The Coupled Damping Coefficients of Symmetric Ships", *Journal of Ship Research*, 5(4), pp 34-55.

Uhlman, J.S., (2001), "A Note on the Development of a Nonlinear Axisymmetric Reentrant Jet Cavitation Model", *ETC Technical Report No.* ETC:RPT:101497/-(U) (Submitted for publication).

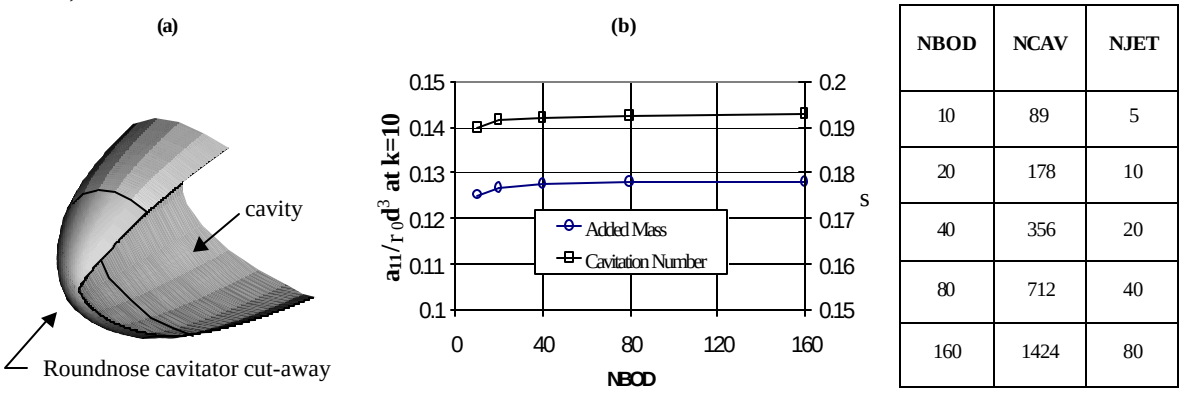

NBOD	NCAV	NJET
10	89	5
20	178	10
40	356	20
80	712	40
160	1424	80

Figure 3. Convergence of surge added mass at k=10 and cavitation number for a roundnose conical cavitator with L/d=5.0 and NBOD=10, 20, 40, 80 and 160. The adjacent table shows the corresponding values of NCAV, NJET.

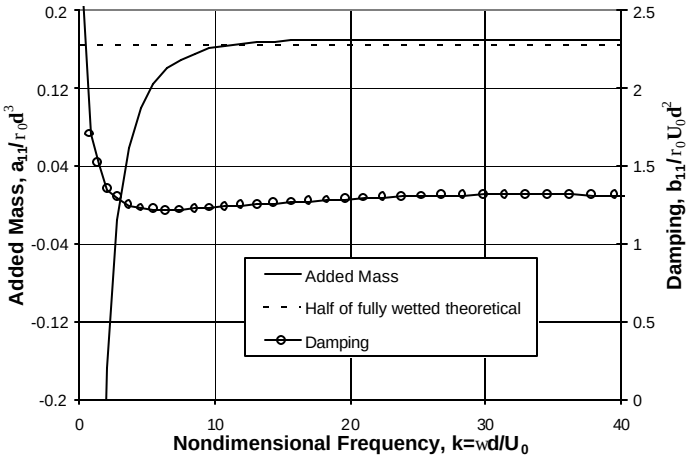

Figure 4. Asymptotic behavior of the surge added mass for a circular disk at high reduced frequency, compared to half the theoretical value for a fully wetted disk.

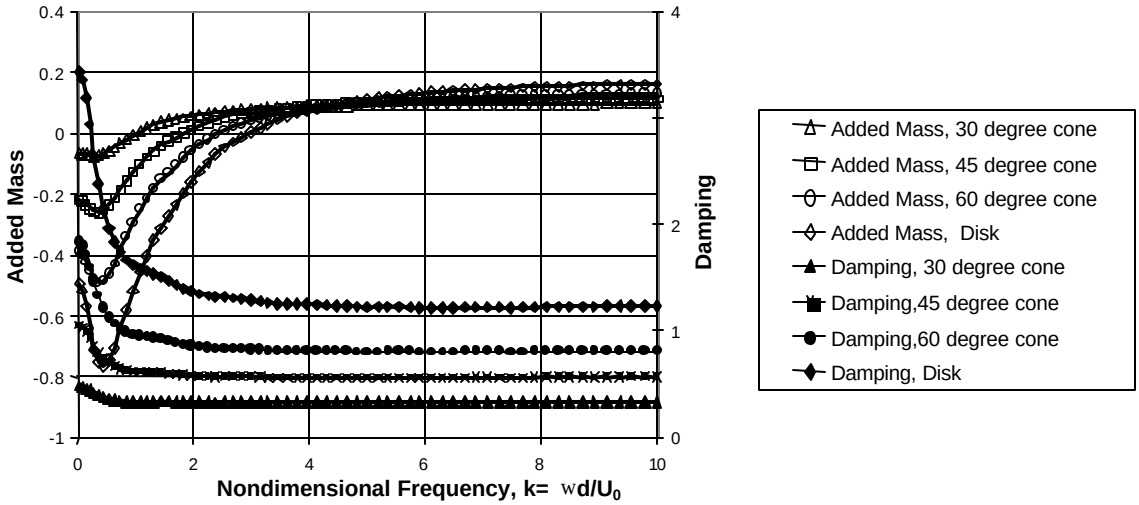

Figure 5. Surge added mass and damping as a function of reduced frequency and cone half-angle for a conical cavitator. The cavity length is held fixed at L/d=5. The added mass is multiplied by $k^2 / r_0 d^3 (1 + k^2)$ and the damping by $1 / r_0 U_0 d^2$.

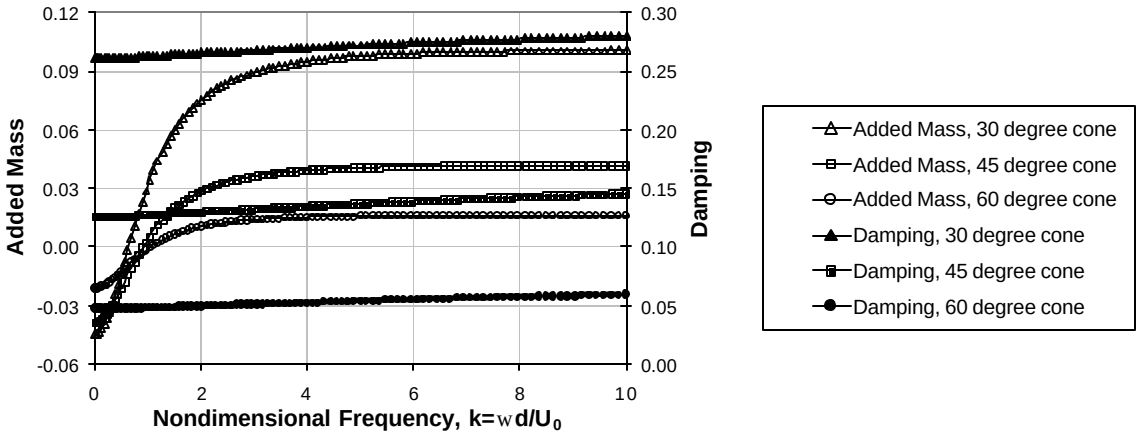

Figure 6. Heave added mass and damping as a function of reduced frequency and cone half-angle for a conical cavitator. The cavity length is held fixed at L/d=5. The added mass is multiplied by $k^2 / r_0 d^3 (1 + k^2)$ and the damping by $1 / r_0 U_0 d^2$.

APPENDIX A. SOURCE AND DIPOLE POTENTIALS FOR AXISYMMETRIC BODIES

A.1 Axial Inflow

Following Uhlman (2001), the source and dipole potentials may be defined in terms of complete elliptic integrals of the first and second kinds. We use a cylindrical coordinate system as shown in figure 7, with $\vec{x} = (x, r, a)$ and $\vec{y} = (x, r, q)$. The Green's function given by equation (23) can then be written

$$G = \frac{1}{\sqrt{(x - x)^2 + r^2 + r^2 - 2r\,r\cos(a - q)}} \tag{41}$$

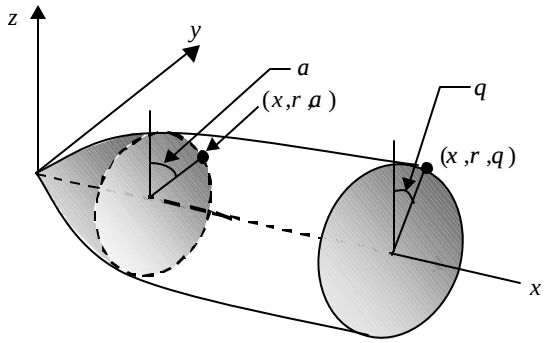

Figure 7. Geometry definitions.

For purely axial inflow, α may be assumed to be zero without loss of generality (Appendix A.2 addresses the case of a non-zero crossflow component). The potential influence at $\vec{x}$ due to a source ring is then

$$\begin{aligned}\Psi &= \int_{-p}^{p} G(\vec{x},\vec{y})\,r\,dq\,a \\ &= \int_{-p}^{p} \frac{r\,dq}{\sqrt{(x-x)^2 + r^2 + r^2 - 2r\,r\cos q}} \\ &= \int_{-p}^{p} \frac{r\,dq}{\sqrt{A - B\cos q}} = r\,J_1^0 = \frac{4r}{\sqrt{A+B}}K(k)\end{aligned} \tag{42}$$

where

$$J_n^m(A,B) = \int_{-p}^{p} \frac{\cos^m(f)}{\left[A - B\cos(f)\right]^{n/2}} df \tag{43}$$

Similarly, the dipole strength is

$$\begin{aligned}\Psi_n &= \int_{-p}^{p} \frac{\partial G(\vec{x},\vec{y})}{\partial n} r\,dq = \int_{-p}^{p} \frac{\partial}{\partial n}\left(\frac{1}{\sqrt{A - B\cos q}}\right) r\,dq \\ &= -\frac{4r(x-x)E(k)n_x}{(A-B)\sqrt{A+B}} - \frac{2\left[(x-x)^2 + (r-r)^2\right]K(k)n_r}{(A-B)\sqrt{A+B}} \\ &\quad + \frac{2\left[(x-x)^2 + r^2 - r^2\right]E(k)n_r}{(A-B)\sqrt{A+B}}\end{aligned} \tag{44}$$

where $K(k)$ and $E(k)$ are first and second kind complete elliptic integrals, respectively (Abramowitz and Stegun, 1970). The quantities A, B and k are defined as follows:

$$\begin{aligned} A &= (x-x)^2 + r^2 + r^2 \\ B &= 2r\,r \\ k &= \sqrt{\frac{2B}{A+B}} \end{aligned} \tag{45}$$

In evaluating the source potential when the field point and integration point coincide (or nearly coincide), it's necessary to consider the logarithmic singularity in the first kind elliptic integral, $K(k)$. From Uhlman (2001), Equation B.7, the logarithmic character of the source potential is explicitly:

$$\Psi = \ln\left(\frac{8r}{\sqrt{s^2 + t^2}}\right)\left[2 - \frac{t}{r} - \frac{s^2 + 2t^2}{4r^2} + O(s^3, t^3)\right] \tag{46}$$

where $s = x - x$ and $t = r - r$. In addition, when the field point lies within the domain of integration, we determine the dipole self-influence using the relation

$$\iint_{S_i} \frac{\partial\Psi}{\partial n} dS = 4p - \iint_{\sum_{i\neq j} S_j} \frac{\partial\Psi}{\partial n} dS\,. \tag{47}$$

Note that the right-hand-side of (47) includes the local 2π contribution to the dipole strength.

A.2 Inflow with a Crossflow Component

When there is a component of the inflow velocity in the crossflow direction, as is the case for heave or pitch motions, the axisymmetric solution may still be applied. For that case, it can be shown that the source and dipole strengths on the boundary are proportional to $\cos q$ (Hess and Smith, 1966). We may then explicitly assume the q dependence by defining the potential as follows

$$j_j = \tilde{f}_j \cos q \tag{48}$$

If we then absorb the $\cos q$ in the definition of the source and dipole potentials, we can show that the original boundary integral equations (equations (39) and (40))

apply, but with $\tilde{j}_j$ in place of j_j and with new definitions for the source and dipole potentials:

$$\Psi = \int_{-p}^{p} \frac{r\cos q\, dq}{\sqrt{A - B\cos q}} = r\, J_1^1(A,B) = \frac{r}{B}\left[AJ_1^0 - J_{-1}^0\right] = \frac{4r}{B}\left[\frac{A}{\sqrt{A+B}}K(k) - \sqrt{A+B}\;E(k)\right] \tag{49}$$

and

$$\Psi_n = \int_{-p}^{p} \frac{\partial}{\partial n}\left(\frac{1}{\sqrt{A - B\cos q}}\right) r\cos q\, dq = n_x \int_{-p}^{p} \frac{\partial}{\partial x}\left(\frac{1}{\sqrt{A - B\cos q}}\right) r\cos q\, dq + n_r \int_{-p}^{p} \frac{\partial}{\partial r}\left(\frac{1}{\sqrt{A - B\cos q}}\right) r\cos q\, dq \tag{50}$$

where

$$\int_{-p}^{p} \frac{\partial}{\partial x}\left(\frac{1}{\sqrt{A - B\cos q}}\right) r\cos q\, dq = r(x - x)\int_{-p}^{p} \frac{\cos q\, dq}{(A - B\cos q)^{3/2}} = r(x - x)J_3^1 = \frac{r(x - x)}{B}\left[AJ_3^0 - J_1^0\right] = \frac{4r(x - x)}{B\sqrt{A+B}}\left[\frac{A}{A - B}E(k) - K(k)\right] \tag{51}$$

and

$$\int_{-p}^{p} \frac{\partial}{\partial r}\left(\frac{1}{\sqrt{A - B\cos q}}\right) r\cos q\, dq = \int_{-p}^{p} \frac{r\, r\cos^2 q - r^2\cos q}{(A - B)^{3/2}} dq = \frac{B}{2}J_3^2 - r^2 J_3^1 = \frac{2E(k)\left[A(A - r^2) - 2r^2 r^2\right]}{r\, r\sqrt{A - B}\,(A - B)} - \frac{2K(k)(A - r^2)}{r\, r\sqrt{A - B}} \tag{52}$$

As before, care must be taken in evaluating the source potential when the field point and integration point coincide (or nearly coincide). Again extracting the logarithmic behavior of the source potential and expanding the multiplier in a Taylor series about $(s,t)=(0,0)$ yields

$$\Psi = \ln\left(\frac{8r}{\sqrt{s^2 + t^2}}\right)\left[2 - \frac{t}{r} + \frac{3s^2 + t^2}{2r^2} + O(s^3, t^3)\right] \tag{53}$$

To obtain the dipole self-influence terms, we note that

$$\frac{\partial G_{cf}}{\partial n} = \frac{\partial G_{axi}}{\partial n} + \frac{\partial H}{\partial n} \tag{54}$$

where G_{cf} is the cross flow Green's function, G_{axi} is the Greens function for axial inflow and H is integrable. We can then write

$$\oiint_S \frac{\partial G_{cf}}{\partial n} dS = \oiint_S \frac{\partial G_{axi}}{\partial n} dS + \oiint_S \frac{\partial H}{\partial n} dS \tag{55}$$

where S is the surface of the complete closed body. The integral on the left hand side can be broken into two components: the integral over the self-influence panel and the integral over the rest of the surface, so that

$$\iint_{S_i} \frac{\partial G_{cf}}{\partial n} dS = \oiint_S \frac{\partial G_{axi}}{\partial n} dS + \oiint_S \frac{\partial H}{\partial n} dS - \sum_{j \neq i} \iint_{S_j} \frac{\partial G_{cf}}{\partial n} dS \tag{56}$$

Furthermore, we can make use of the fact that

$$\oiint_S \frac{\partial G_{axi}}{\partial n} dS = 4p \tag{57}$$

so that

$$\iint_{S_i} \frac{\partial G_{cf}}{\partial n} dS = 4p + \oiint_S \frac{\partial H}{\partial n} dS - \sum_{j \neq i} \iint_{S_j} \frac{\partial G_{cf}}{\partial n} dS \tag{58}$$

The second term on the right-hand-side of (58) can be written

$$\oiint_S \frac{\partial H}{\partial n} dS = n_x \oiint_S \frac{\partial H}{\partial x} dS + n_r \oiint_S \frac{\partial H}{\partial r} dS \tag{59}$$

To evaluate this exp ression, we note that

$$\int_{-p}^{p} \frac{\partial}{\partial x}\left(\frac{\cos q - 1}{\sqrt{A - B\cos q}}\right) r\cos q\, dq = r(x - x)\left[J_3^1 - J_3^0\right] = \frac{2(x - x)}{r\sqrt{A+B}}\left[E(k) - K(k)\right] \tag{60}$$

and

$$\int_{-p}^{p} \frac{\partial}{\partial r}\left(\frac{\cos q - 1}{\sqrt{A - B\cos q}}\right) r\cos q\, dq$$
$$= rr\left[J_3^2 - J_3^1\right] - r^2\left[J_3^1 - J_3^0\right]$$
$$= \frac{\left(B + 2(A - r^2)\right)E(k)}{rr\sqrt{A+B}} - \frac{\left(B - 2(A - r^2)\right)K(k)}{rr\sqrt{A+B}} \tag{61}$$

Special treatment is also required to evaluate these expressions when the field point and integration point are close to one another to ensure that the logarithmic behavior of the second kind elliptic integral is accurately captured.

APPENDIX B. COMPUTATION OF THE GENERALIZED NORMAL AND THE M-TERMS

The generalized normal and m -terms take the form

$$\begin{aligned}
&(n_1, n_2, n_3) = \hat{n} \\
&(n_4, n_5, n_6) = \vec{x}\times\hat{n} \\
&(m_1, m_2, m_3) = -\hat{n}\cdot\nabla(\nabla\Phi_0) \\
&(m_4, m_5, m_6) = -\hat{n}\cdot\nabla[\vec{x}\times\nabla\Phi_0]
\end{aligned} \tag{62}$$

where $\vec{x} = (x, y, z) = (x, r\sin q, r\cos q)$. In order to compute these terms for the axisymmetric case we note that the velocities satisfy the continuity equation

$$\frac{\partial u}{\partial x} + \frac{\partial u_r}{\partial r} + \frac{u_r}{r} = 0 \tag{63}$$

and the condition of irrotationality

$$\frac{\partial u_r}{\partial x} - \frac{\partial u}{\partial r} = 0\,. \tag{64}$$

In (63) and (64) we've introduced the three velocity components

$$\nabla\Phi_0 = (u, v, w) = (u, u_r\sin q, u_r\cos q)\,.$$

For axisymmetric bodies, we also note that the unit normal may be written

$$\hat{n} = \frac{\partial r}{\partial s}\hat{i} - \frac{\partial x}{\partial s}\hat{j} \tag{65}$$

so that

$$\hat{n}\cdot\hat{n} = \left(\frac{\partial x}{\partial s}\right)^2 + \left(\frac{\partial r}{\partial s}\right)^2 = 1 \tag{66}$$

Employing these relations with the chain rule expansions

$$\begin{aligned}
\frac{\partial u}{\partial s} &= \frac{\partial u}{\partial x}\frac{\partial x}{\partial s} + \frac{\partial u}{\partial r}\frac{\partial r}{\partial s} \\
\frac{\partial u_r}{\partial s} &= \frac{\partial u_r}{\partial x}\frac{\partial x}{\partial s} + \frac{\partial u_r}{\partial r}\frac{\partial r}{\partial s}
\end{aligned} \tag{67}$$

we obtain the following expressions:

$$\begin{aligned}
\frac{\partial u}{\partial x} &= \frac{\partial u}{\partial s}\frac{\partial x}{\partial s} - \left(\frac{\partial u_r}{\partial s} + \frac{u_r}{r}\frac{\partial r}{\partial s}\right)\frac{\partial r}{\partial s} \\
\frac{\partial u}{\partial r} &= \left(\frac{\partial u_r}{\partial s} + \frac{u_r}{r}\frac{\partial r}{\partial s}\right)\frac{\partial x}{\partial s} + \frac{\partial u}{\partial s}\frac{\partial r}{\partial s}
\end{aligned} \tag{68}$$

and

$$\begin{aligned}
\frac{\partial u_r}{\partial x} &= \frac{\partial u_r}{\partial s}\frac{\partial x}{\partial s} + \left(\frac{\partial u}{\partial s} + \frac{u_r}{r}\frac{\partial x}{\partial s}\right)\frac{\partial r}{\partial s} \\
\frac{\partial u_r}{\partial r} &= \frac{\partial u_r}{\partial s}\frac{\partial r}{\partial s} - \left(\frac{\partial u}{\partial s} + \frac{u_r}{r}\frac{\partial x}{\partial s}\right)\frac{\partial x}{\partial s}
\end{aligned} \tag{69}$$

The required motions for the axisymmetric base case are surge, heave and pitch. The expressions for the generalized normal and m-terms are shown in Table 1. The m-terms are evaluated numerically with the help of equations (68) and (69).

Table 1 *Definition of the generalized normal and m-terms for j=1, 3 and 5.*

	Generalized normal, n_j	**M-term, m_j**
Surge	$n_1 = n_x$	$m_1 = -\hat{n}\cdot\nabla u = -\left(n_x\frac{\partial u}{\partial x} + n_r\frac{\partial u}{\partial r}\right)$
Heave	$n_3 = n_z = n_r\cos q$	$m_3 = -\hat{n}\cdot\nabla w = -\hat{n}\cdot\nabla[u_r\cos q] = -\left(n_x\frac{\partial u_r}{\partial x} + n_r\frac{\partial u_r}{\partial r}\right)\cos q$
Pitch	$n_5 = zn_x - xn_z = (m_x - xn_r)\cos q$	$m_5 = -\hat{n}\cdot\nabla(zu - xw) = -\hat{n}\cdot\nabla[(ru - xu_r)\cos q] = -\left\{n_x\left[r\frac{\partial u}{\partial x} - u_r - x\frac{\partial u_r}{\partial x}\right] + n_r\left[u + r\frac{\partial u}{\partial r} - x\frac{\partial u_r}{\partial r}\right]\right\}\cos q$

APPENDIX C. A DISCUSSION OF THE THEODORSEN HEAVE PROBLEM

C.1 Background

In this appendix, the unsteady lift force on a heaving flat plate hydrofoil is expressed in terms of added mass and damping coefficients as functions of reduced frequency, using the classical result of Theodorsen. With the force formulated in this manner, we can show that the added mass coefficient is negative for low reduced frequency, as it is for the case of the supercavitating bodies discussed in the main body of this paper.

C.2 Formulation

Consider a flat plate hydrofoil whose chord lies on the segment of the x-axis $-1 < x < 1$. The lift force acting on the foil is given by (see, for instance, Newman, 1986)

$$\begin{aligned} L = &-2\pi\rho U_0^2 C(k)\left[ikh_0 - \left(1+\tfrac{1}{2}ik\right)a_0\right]e^{i\omega t} \\ &-\pi\rho\left[-\omega^2 h_0 - i\omega U_0 a_0\right]e^{i\omega t} \end{aligned} \tag{70}$$

where the heave and pitch functions are given by

$$\begin{aligned} h(t) &= \mathrm{Re}\left[h_0 e^{i\omega t}\right] \\ a(t) &= \mathrm{Re}\left[a_0 e^{i\omega t}\right] \end{aligned} \tag{71}$$

The lift for the pure heave problem is then

$$L = -2\pi\rho U_0^2 C(k)\left[ikh_0\right]e^{i\omega t} + \pi\rho_0\left[\omega^2 h_0\right]e^{i\omega t} \tag{72}$$

where $C(k)$ is the Theodorsen function, ρ_0 is the fluid density, and U_0 is the free-stream velocity. The Theodorsen function is given by

$$C(k) = \frac{H_1^{(2)}(k)}{H_1^{(2)}(k) + iH_0^{(2)}(k)} \tag{73}$$

where $H_0^{(2)}(k)$ and $H_1^{(2)}(k)$ are the second kind Hankel functions of orders zero and one, respectively. If we then denote the lift by

$$L = \left[L_R + iL_I\right]e^{i\omega t} \tag{74}$$

we find that

$$\begin{aligned} L_R &= 2\pi\rho_0 U_0^2\left[C_I(k)k + \tfrac{1}{2}k^2\right]h_0 \\ L_I &= 2\pi\rho_0 U_0^2\left[-C_R(k)k\right]h_0 \end{aligned} \tag{75}$$

The reduced frequency is defined as

$$k = \frac{\omega}{U}.$$

The lift, L, may now be written in terms of the added mass and damping coefficients (a and b, respectively) as follows:

$$L = \rho U^2\left(k^2 a - ikb\right)h_0 \tag{76}$$

where

$$\begin{aligned} a &= \pi\left[1 + \frac{2}{k}C_I(k)\right] \\ b &= 2\pi C_R(k) \end{aligned} \tag{77}$$

The added mass and damping coefficients are shown in Figure 8. As shown in the figure, the added mass for a heaving hydrofoil can be negative for small values of the reduced frequency. The physical explanation of the phenomenon is similar to that described in Section 2.5 for the supercavitating disk in surge. It should be noted that, while the added mass is negative and singular as the reduced frequency tends to zero, the added mass force actually is finite and and vanishes at zero reduced frequency. This is shown in Figure 8, where the added mass is shown multiplied by the square of the reduced frequency, which is directly proportional to the added mass force.

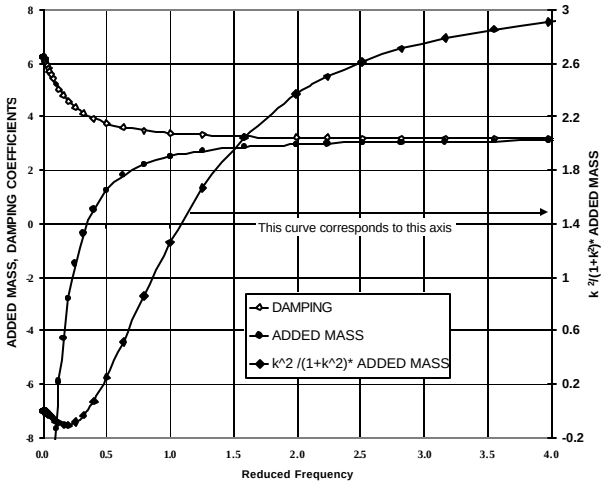

Figure 8. Added mass and damping for a heaving flat-plate hydrofoil.